Earthquakes and Structures, *Vol. 12, No. 1 (2017) 135-144*
DOI: https://doi.org/10.12989/eas.2017.12.1.135

Nonlinear response of r.c. framed buildings retrofitted by different base-isolation systems under horizontal and vertical components of near-fault earthquakes

Fabio Mazza*, Mirko Mazza[a] and Alfonso Vulcano[b]

Dipartimento di Ingegneria Civile, Università della Calabria, Rende (Cosenza), Italy

(Received July 16, 2016, Revised October 25, 2016, Accepted December 12, 2016)

Abstract. Near-fault ground motions are characterized by high values of the ratio between the peak of vertical and horizontal ground accelerations, which can significantly affect the nonlinear response of a base-isolated structure. To check the effectiveness of different base-isolation systems for retrofitting a r.c. framed structure located in a near-fault area, a numerical investigation is carried out analyzing the nonlinear dynamic response of the fixed-base and isolated structures. For this purpose, a six-storey r.c. framed building is supposed to be retrofitted by insertion of an isolation system at the base for attaining performance levels imposed by current Italian code in a high-risk seismic zone. In particular, elastomeric (e.g., high-damping-laminated-rubber bearings, HDLRBs) and friction (e.g., steel-PTFE sliding bearings, SBs, or friction pendulum bearings, FPBs) isolators are considered, with reference to three cases of base isolation: HDLRBs acting alone (i.e., EBI structures); in-parallel combination of HDLRBs and SBs (i.e., EFBI structures); FPBs acting alone (i.e., FPBI structures). Different values of the stiffness ratio, defined as the ratio between the vertical and horizontal stiffnesses of the HDLRBs, sliding ratio, defined as the global sliding force divided by the maximum sliding force of the SBs, and in-plan distribution of friction coefficient for the FPs are investigated. The EBI, EFBI and FPBI base-isolation systems are designed assuming the same values of the fundamental vibration period and equivalent viscous damping ratio. The nonlinear dynamic analysis is carried out with reference to near-fault earthquakes, selected and scaled on the design hypotheses adopted for the test structures.

Keywords: r.c. base-isolated structures; elastomeric bearings; friction bearings; nonlinear dynamic analysis; near-fault ground motions

1. Introduction

The seismic vulnerability of existing reinforced concrete (r.c.) framed buildings is mainly due to degradation of the material properties and low building standards. Brittle mechanism represents a typical problem in r.c. frame members designed in line with out-of-date seismic codes, where capacity design criteria to avoid brittle failure modes were not provided (Calvi 2013, Mazza 2015, Mazza and Pucci 2016). A lot of mechanical-empirical formulations, calibrated in accordance with experimental data, is available to evaluate brittle mechanism at section (De Luca and Verderame 2013) and joint (Favvata *et al*. 2008, 2014, Lima *et al*. 2012) levels. Retrofitting strategies that can be used to eliminate possible sources of brittle failures of an existing building are those based on the total or local r.c. jacketing of frame members and beam-column joints (Chalioris *et al*. 2008, Karayannis *et al*. 2008, Tsonos 2007, 2010, 2014). Moreover, irregularities in elevation due to soft-storeys or unsymmetrical layout of infill walls can produce significant variations in stiffness, strength and mass distribution of existing r.c. framed buildings (Karayannis *et al*. 2011), leading to severe seismic damage. To mitigate these effects and retrofit the structure, base-isolation systems can be suitably inserted in the framed structure. Different isolation strategies or their combination can be used, allowing considerable reduction of the horizontal seismic loads transmitted to the superstructure (Naeim and Kelly 1999, Mazza *et al*. 2012, Mazza and Mazza 2016, Baratta *et al*. 2012, Sorace and Terenzi 2014): more precisely, increasing the fundamental vibration period of the structure, to shift it in the range of low spectral accelerations; limiting the maximum horizontal force transmitted to the superstructure, depending on the friction coefficient. Therefore, the base-isolation systems are usually made with elastomeric bearings (e.g., HDLRBs), sometimes coupled in hybrid combination with steel-PTFE sliding bearings (SBs), or frictional pendulum bearings (FPBs). It is worth noting that in the case of an in-parallel combination of HDLRBs and SBs (i.e., EFBI structure) or FPBs acting alone (i.e., FPBI structure), the base-isolated structure, under particular conditions, behaves as a fixed-base structure: i.e., in the

*Corresponding author, Researcher
E-mail: fabio.mazza@unical.it
[a]Ph.D.
E-mail: mirko.mazza@unical.it
[b]Full Professor
E-mail: alfonso.vulcano@unical.it

ISSN: 2092-7614 (Print), 2092-7622 (Online)

horizontal direction, until the friction threshold of the sliding bearings is not exceeded; in the vertical direction, providing the grid of girders placed at the top of the isolation system with a high stiffness and avoiding uplifts of the SBs or FPs. Moreover, in the case of elastomeric bearings acting alone (i.e., EBI structure), the superstructure behaves as isolated or practically fixed-base along the vertical direction depending on the value, respectively very low or very high, of the ratio α_{K0}(=K_{V0}/K_{H0}) between the vertical (K_{V0}) and horizontal (K_{H0}) nominal stiffnesses of the isolation system.

A considerable increase of deformability of an isolated structure, in comparison with that of the corresponding fixed-base structure, may lead to an amplification in the structural response under strong near-fault ground motions, which are characterized by long-duration horizontal pulses. In particular, the frequency content of the motion transmitted by the isolators to the superstructure can become critical for the superstructure when the pulse intensity is such that the superstructure undergoes plastic deformations; also, an amplification in the structural response is possible due to the long duration of the pulse (Mazza and Vulcano 2012, Mazza 2015, Foti 2014). Moreover, near-fault ground motions are characterized by high values of the ratio α_{PGA} between the peak value of the vertical acceleration (PGA_V) and the analogous value of the horizontal acceleration (PGA_H), which can become critical for a base-isolated structure. More specifically, high values of α_{PGA} can notably modify the axial load in r.c. columns and the ductility demand along the span of the beams (Mazza 2016), while elastomeric and sliding bearings can undergo tensile loads and uplifts (Kasalanati and Constantinou 2005), respectively.

The above considerations point out the importance of checking the effectiveness of different isolation systems for retrofitting a r.c. framed structure. For this purpose, a numerical investigation is carried out with reference to a six-storey r.c. framed building, which, primarily designed (as to be a fixed-base one) in compliance with an old Italian seismic code (DM96 1996) for a medium-risk zone, has to be retrofitted by insertion of an isolation system at the base for attaining performance levels imposed by the current Italian code (NTC08 2008) in a high-risk seismic zone. Besides the (fixed-base) primary structure, three cases of base isolation are studied: HDLRBs acting alone (i.e., EBI structure); in-parallel combination of HDLRBs and SBs (i.e., EFBI structure); FPBs acting alone (i.e., FPBI structure). The nonlinear analysis of the fixed-base and base-isolated structures is carried out considering the horizontal components of seven near-fault ground motions selected in the Pacific Earthquake Engineering Research center database (PEER 2008) and scaled on the basis of the design hypotheses adopted for the test structure.

2. Design and modelling of the fixed-base original structure

A typical six-storey residential building with r.c. framed structure, whose symmetric plan is shown in Fig. 1, is

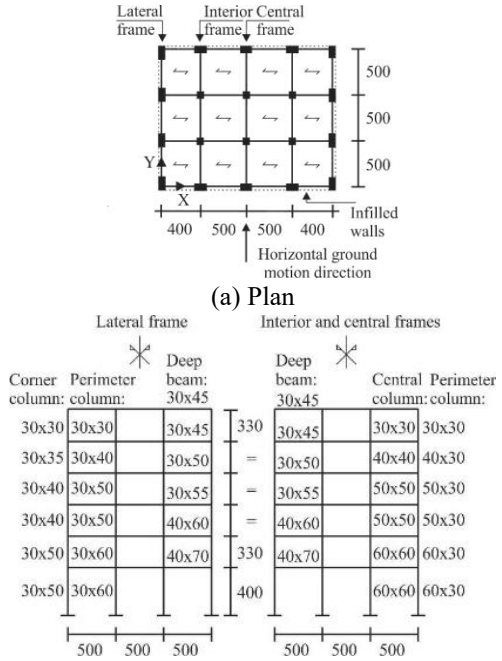

(a) Plan

(b) Elevations in the Y direction

Fig. 1 Fixed-base original structure (units in cm)

considered as test structure. Masonry infill walls are considered as nonstructural elements regularly distributed along the perimeter (Fig. 1(a)) and in elevation. A simulated design of the original framed building is carried out in accordance with the previous Italian code (DM96 1996), for a medium-risk seismic region (seismic coefficient: C=0.07) and a typical subsoil class (main coefficients: R=ε=β=1). The gravity loads for the r.c. framed structure are represented by a dead load of 4.2 kN/m^2 on the top floor and 5.0 kN/m^2 on the other floors, and a live load of 2.0 kN/m^2 on all the floors; an average weight of about 2.7 kN/m^2 is considered for the masonry infill walls. Concrete cylindrical compressive strength of 25 N/mm^2 and steel reinforcement with yield strength of 375 N/mm^2 are considered.

The geometric dimensions of the lateral, interior and central frames are shown in Fig. 1(b), where cross section of deep beams and columns (i.e., corner, perimeter and central) are also reported. The design is carried out to comply with the ultimate limit states. Detailing for local ductility is also imposed to satisfy minimum conditions for the longitudinal bars of the r.c. frame members: for the beams, a tension reinforcement ratio nowhere less than 0.37% is provided and a compression reinforcement not less than half of the tension reinforcement is placed at all sections; for a section of each column a minimum steel geometric ratio of 1% is assumed, supposing that the minimum reinforcement ratio corresponding to one side of the section be about 0.35%. Finally, the fundamental vibration period and effective mass, expressed as percentage of the total mass (m_{tot}=1634 kNs^2/m), along the ground motion direction (i.e., Y direction in Fig. 1(a)) are T_{1H}=0.665 s and m_{E1}=76% m_{tot}, respectively.

The r.c. frame members are idealized by means of a two-component model, constituted of an elastic-plastic

component and an elastic component, assuming a bilinear moment-curvature law. The effect of the axial load on the ultimate bending moment of the columns (M-N interaction) is also considered, assuming fully elastic both the axial and shear strains. At each step of the analysis, the elastic-plastic solution is evaluated in terms of the initial state and the incremental load on the basis of a holonomic law, as a solution of the Haar-Kàrmàn principle (Mazza and Vulcano 2010). More specifically, by imposing plastic conditions on the bending moments (m_i and m_j) at the end sections (i and j) of each frame element, the elastic-plastic solution can be obtained considering, among the equilibrated internal forces $\mathbf{m}=(m_i, m_j)^T$, the one resulting closest to the elastic solution $\mathbf{m}_E=(m_{Ei}, m_{Ej})^T$ and satisfying the complementary energy minimum condition for the self-equilibrated internal forces ($\mathbf{m}$-$\mathbf{m}_E$). The above solution can be easily obtained by using the three-step algorithm illustrated in Fig. 2, where M_{y1} (M_{y4}) and M_{y3} (M_{y2}) represent, respectively, the yield moments producing tension at top and bottom of the end section i (j). For the sake of simplicity, only the horizontal ground motion component indicated in Fig. 1(a) is considered for the test structures examined in the numerical investigation. To account for the plastic deformations along the beams induced by the vertical component of the ground motions, each of them is discretized into (four) sub-elements, each corresponding to a given longitudinal reinforcement. At each step of the analysis, plastic conditions are checked at the potential critical sections of the beams (i.e., end, quarter-span and mid-span sections) and columns (i.e., end sections).

The dynamical equilibrium equations, e.g., in the case of a plane structure subjected to the horizontal ($\ddot{u}_g$) and vertical ($\ddot{w}_g$) components of the ground motion, can be expressed as

$$\mathbf{M}\ddot{\mathbf{u}}(t)+\mathbf{C}\dot{\mathbf{u}}(t)+\mathbf{f}\left[\mathbf{u}(t)\right]=-\mathbf{M}\left[\mathbf{i}_h\ddot{u}_g(t)+\mathbf{i}_v\ddot{w}_g(t)\right] \quad (1)$$

which represents a nonlinear implicit system containing the unknown velocity vector $\dot{\mathbf{u}}$, being: $\mathbf{M}$ the mass matrix, $\mathbf{u}$ and $\ddot{\mathbf{u}}$ the displacement and acceleration vectors, $\mathbf{f}$ the structural reaction vector, $\mathbf{i}_h$ and $\mathbf{i}_v$ the vectors of the influence coefficients along the horizontal and vertical directions, respectively. According to the Rayleigh hypothesis, the damping matrix $\mathbf{C}$ is assumed to be a linear combination of the mass and the stiffness matrices, assuming a suitable damping ratio associated with two control frequencies (or modes). The solution of Eq. (1) is obtained by the following residual iteration scheme

$$\mathbf{r}^{(j)}=\mathbf{q}_1^{(j)}-\mathbf{q}_0+\left(\frac{1}{2}-\alpha\right)\Delta t\left(\mathbf{s}_0-\mathbf{p}_0\right)+\left(\frac{1}{2}+\alpha\right)\Delta t\left(\mathbf{s}_1^{(j)}-\mathbf{p}_1\right) \quad (2)$$

$$\dot{\mathbf{u}}_1^{(j+1)}=\dot{\mathbf{u}}_1^{(j)}-\mathbf{H}\mathbf{r}^{(j)} \quad (3)$$

in which indexes 0 and 1 refer, respectively, to the beginning and the end of the generic time step, $\mathbf{q}=\mathbf{M}\dot{\mathbf{u}}$ is the momentum vector, $\mathbf{s}=\mathbf{f}[\mathbf{u}]+\mathbf{C}\dot{\mathbf{u}}$, while α and β are suitable functions of the time step Δt. The convergence of the iterative process is assured adopting the iteration matrix

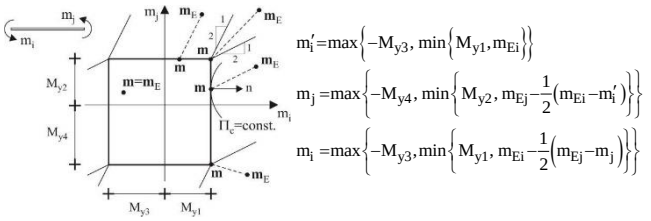

Fig. 2 Elastic-plastic solution of r.c. frame member according to the Haar-Kàrmàn principle

$$\mathbf{H}=\left\{\mathbf{M}+\left(\frac{1}{2}+\alpha\right)\left(\frac{1}{2}+\beta\right)\Delta t^2\mathbf{K}_E+\left(\frac{1}{2}+\alpha\right)\Delta t\mathbf{C}\right\}^{-1} \quad (4)$$

where $\mathbf{K}_E$ is the elastic stiffness matrix.

3. Design and modelling of the base-isolated retrofitted structures

To retrofit the six-storey original (fixed-base) framed building, for attaining performance levels imposed by the current Italian code (NTC08 2008) in a high-risk seismic zone (peak ground acceleration on rock, a_g=0.262 g at the life-safety limit state) and medium subsoil class (class C, site amplification factor S=1.319), three in-plan configurations of elastomeric and sliding bearings are considered: (a) EBI structure, with elastomeric bearings acting alone (i.e., high-damping-laminated-rubber bearings, HDLRBs type 1); (b) EFBI structure, with an in-parallel combination of elastomeric (i.e., HDLRBs type 2) and friction (i.e., steel-PTFE sliding bearings, SBs) bearings; (c) FPBI structure, with friction pendulum bearings (i.e., FPBs) acting alone. A sketch of the HDLRB, SB and FPB installation below a column of the original structure is shown in Fig. 3. It is assumed that would be possible to temporarily hold up the whole structure and to create an independent foundation, in order to link the isolators to the double foundation system constituted of the existing and new foundations. A seismic gap needs to be realized around the building, whose function is to allow the base-isolation

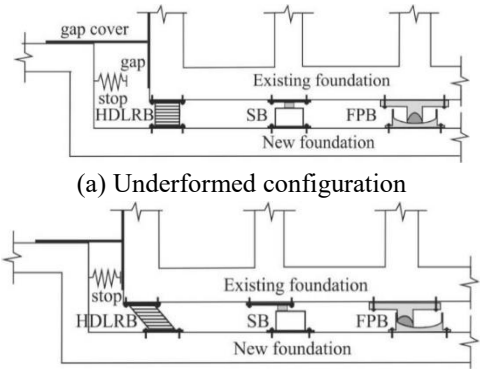

Fig. 3 Sketch of the installation of isolators below columns of the original structure

Table 1 Properties and results of verifications for HDLRB type 1 acting alone (units in kN, cm and s)

α_{K0}	T_{1V}	K_{H0}	K_{V0}	C_H	C_V	D	t_e	S_1	S_2	E_c	γ_s	γ_{tot}	$(P_{cr}/P)_{min}$
800	0.088	6.77	5420	0.97	7.69	70	22.6	13.24	3.05	32.9	1.03	3.34	2.00
1200	0.072	6.77	8129	0.97	9.32	64	18.9	18.74	3.20	53.9	1.24	3.66	2.00
1600	0.062	6.77	10839	0.97	10.7	53	13.3	22.02	3.98	65.6	1.76	4.76	2.00
2000	0.056	6.77	13549	0.97	12.1	53	13.3	26.73	4.03	80.0	2.00	4.16	2.56

horizontal movements during an earthquake, while a stop, to limit excessive movements, and crawl spaces for inspection and maintenance of the base-isolation system should be considered.

An additional mass of 511 kNs^2/m, placed above the isolation level, is assumed at the level of the rigid girders, with a cross section of 50×100 cm^2. The base-isolation systems are designed assuming the same values of the fundamental vibration period (i.e., T_{1H}=2.5 s) and equivalent viscous damping ratio (i.e., ξ_H=18%). Finally, the (horizontal) design spectral displacement at the NTC08 collapse limit state is assumed equal to 23.33 cm.

3.1 Elastomeric Base-Isolated (EBI) structures

The design of the twenty HDLRBs type 1 of the EBI structure shown in Fig. 4, which are simply assumed with the same dimensions so as to obtain a larger torsional stiffness, is carried out according to the prescriptions imposed by NTC08 at the collapse limit state. Four values of the nominal stiffness ratio of the isolation system, defined as the ratio between the horizontal (K_{H0}) and vertical (K_{V0}) nominal stiffnesses of the HDLRBs, are considered (i.e., α_{K0}=800, 1200, 1600 and 2000).

A shear modulus G=0.4 MPa and a volumetric compression modulus E_b=2000 MPa are assumed for the elastomer. The HDLRBs fulfill the ultimate limit state verifications regarding the maximum shear strains: i.e., $\gamma_{tot}=\gamma_s+\gamma_c+\gamma_\alpha \le 5$ and $\gamma_s \le 2$, where γ_{tot} represents the total design shear strain, while γ_s, γ_c and γ_α represent the shear strains of the elastomer due to seismic displacement, axial compression and angular rotation, respectively. Moreover, the maximum compression axial load (P) does not exceed the critical load (P_{cr}) divided by a safety coefficient equal to 2.0. The maximum allowable tensile stress (σ_{tu}) is assumed as 2G (=0.8 MPa).

In Table 1, depending on stiffness ratios α_{K0} considered in the analysis, the base isolation system properties are reported: i.e., the fundamental vibration period in the vertical direction (T_{1V}), the horizontal (K_{H0}) and vertical (K_{V0}) nominal stiffnesses and the corresponding equivalent damping coefficients (C_H and C_V), assuming an equivalent viscous damping ratio in the horizontal direction, ξ_H, equal to 18%, and an analogous ratio in the vertical direction, ξ_V, equal to 5%. The following geometrical and mechanical properties of the HDLRBs are also reported in Table 1: the diameter of the isolator (D); the total thickness of elastomer (t_e); primary (S_1) and secondary (S_2) shape factors; compression modulus (E_c). In Table 1 the results of the verifications for the HDLRBs are also reported. It is interesting to note that the design of the isolators resulted

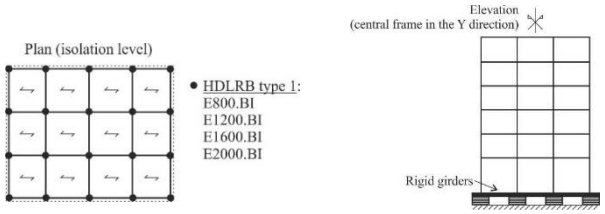

(a) (b)

Fig. 4 EBI structures: HDLRBs type 1 acting alone

mainly depending on the conditions imposed on the minimum value of P_{cr}/P (i.e., E800.BI, E1200.BI and E1600.BI) and maximum value of γ_s (i.e., E2000.BI). No tensile forces are found in the isolators.

Experimental results (Ryan *et al.* 2004) pointed out that the horizontal stiffness of a HDLRB (starting from K_{H0}) decreases with increasing vertical load (P), while the corresponding vertical stiffness (starting from K_{V0}) decreases with increasing lateral deformation (u_H). To account for the observed behaviour, the two-spring-two-dashpot model shown in Fig. 5(a), constituted of a nonlinear spring acting in parallel with a linear viscous dashpot both in the horizontal and vertical directions, can be adopted (Mazza and Vulcano 2012). The nonlinear force-displacement laws for the horizontal (F_K-u_H) and vertical (P-u_V) springs (Fig. 5(b)) are

$$F_K = K_H u_H = K_{H0}\left[1-\left(P/P_{cr}\right)^2\right]u_H, \tag{5a}$$

$$P_K = K_V\left(u_V - \frac{\alpha_b}{\alpha_{K0}}\frac{16}{\pi^2 D S_2}u_H^2\right) \tag{5b}$$

where $\alpha_b=h_b/t_r$, h_b being the total height of the bearing. Moreover, the linear force-velocity laws for the horizontal (F_C-$\dot{u}_H$) and vertical (P_C-$\dot{u}_V$) dashpots in Fig. 5(a) are expressed as

$$F_C = C_H\dot{u}_H \cong \left(\xi_H K_{H0} T_{1H}/\pi\right)\dot{u}_H, \tag{6a}$$

$$P_C = C_V\dot{u}_V \cong \left(\xi_V K_{V0} T_{1V}/\pi\right)\dot{u}_V \tag{6b}$$

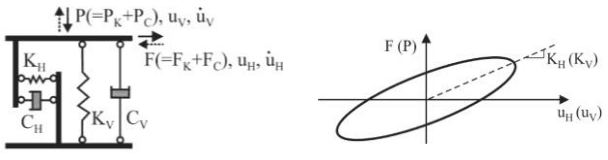

(a) (b)

Fig. 5 Modelling of the base-isolation system for the EBI structure: HDLRBs acting alone

3.2 Elastomeric and Friction Base-Isolated (EFBI) structures

The design of the in-parallel combination of HDLRBs type 2 and steel-PTFE SBs for the EFBI structure is carried out in order to increase the secondary shape factor of the elastomeric bearings (e.g., $S_2 \geq 4$ is a conservative assumption against buckling) in comparison with HDLRBs type 1 shown in Table 1. To this end, three arrangements of elastomeric and sliding bearings are considered in Fig. 6: i.e., four interior SBs (S4), four interior and two perimeter SBs (S6) and six interior and two perimeter SBs (S8). Each solution corresponds to a value of the nominal sliding ratio $\alpha_{S0}(=F_{S0}/F_{S0,max})$ of the SBs under gravity loads, defined as the global sliding force (F_{S0}) divided by the maximum sliding force ($F_{S0,max}$); this latter one evaluated supposing that sliding bearings are placed under each column of the test structure. The same nominal stiffness ratios adopted for the EBI structures (i.e., α_{K0}=800, 1200, 1600 and 2000) are assumed in this case for the HDLRBs type 2.

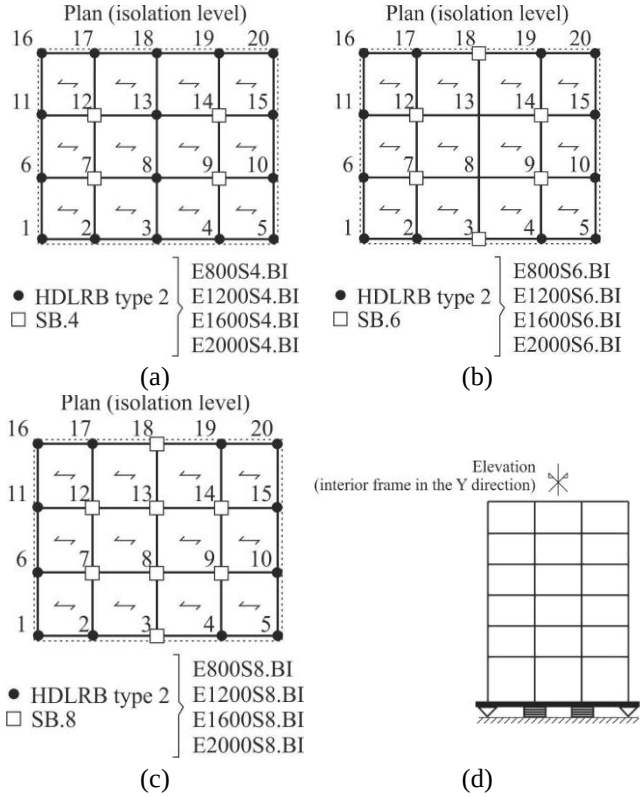

Fig. 6 EFBI structures: in-parallel combination of HDLRBs type 2 and SBs

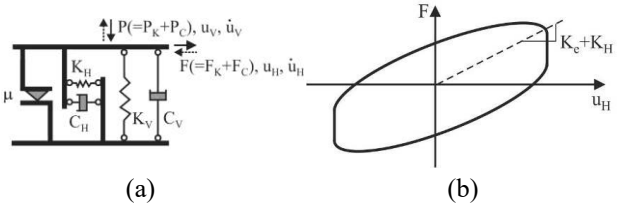

Fig. 7 Modelling of the base-isolation system for the EFBI structure

The equivalent viscous damping in the horizontal direction (ξ_H), for the in-parallel combination of HDLRBs and SBs (Fig. 7), is evaluated as

$$\xi_H = \frac{W_{h,HDLRBs} + W_{h,SBs}}{4\pi\left(W_{s,HDLRBs} + W_{s,SBs}\right)} = \xi_{H,HDLRBs} + \xi_{H,SBs} \quad (7)$$

where W_s represents the strain energy

$$W_{s,HDLRBs} = \frac{1}{2}\sum_{i=1}^{n_{HDLRBs}} K_{Hi} \times u_H^2 \quad (8a)$$

$$W_{s,SBs} = \frac{1}{2}\sum_{i=1}^{n_{SBs}} K_{ei} \times u_H^2 = \frac{1}{2}\sum_{i=1}^{n_{SBs}} \mu_{max} \times P_i \times u_H \quad (8b)$$

and W_h the hysteretic energy

$$W_{h,HDLRBs} = 4\pi W_{s,HDLRBs} \times \xi_{H,HDLRBs}, \quad (9a)$$

$$W_{h,SBs} = \sum_{i=1}^{n_{SBs}} 4\mu_{max} \times P_i \times u_H \quad (9b)$$

being K_{ei} the effective (secant) stiffness of a SB, at the horizontal displacement u_H, and μ_{max} the dynamic-fast coefficient of friction.

The coefficient of friction at sliding velocity $\dot{u}_H$ is evaluated as (Constantinou *et al.* 1990)

$$\mu = \mu_{max} - \left(\mu_{max} - \mu_{min}\right)e^{-\alpha\dot{u}_H} \quad (10)$$

which attains the value μ_{max} or μ_{min} respectively at very high or very low velocity, while α is a constant for given values of pressure and temperature.

Equivalent viscous damping ratios of elastomeric ($\xi_{H,HDLRBs}$) and sliding ($\xi_{H,SBs}$) bearings are calculated in accordance with Eqs. (7)-(9), referring to the (horizontal) spectral displacement at the collapse limit state (i.e., S_d=23.33 cm) and considering the gravity loads and a dynamic-fast sliding friction coefficient μ_{max}=4.2%. Finally, the equivalent viscous damping ratio of the HDLRBs type 2 in the vertical direction is assumed equal to ξ_V=5%. Main properties of the HDLRBs type 2 are reported in Tables 2(a)-2(c). It is noteworthy that the design of the elastomeric bearings has been generally limited by the condition imposed on the maximum tensile stress (i.e., $(\sigma_t/\sigma_{tu})_{max}$). Dynamic properties of the SBs are reported in Table 3.

The nonlinear dynamic analysis will be carried out assuming μ_{max}/μ_{min}=2.5 and a rate parameter α (see Eq. (1)) equal to 5.5 s/m, according to experimental results (Dolce *et al.* 2005). The SB response basically depends on sliding velocity, contact pressure and temperature (Constantinou *et al.* 1990, Dolce *et al.* 2005, Lomiento *et al.* 2013, Fagà *et al.* 2016). More specifically, the coefficient of sliding friction increases with increasing velocity up to a certain velocity value, beyond which it remains almost constant, while drops with increasing pressure (with a rate of

Table 2(a) Properties and results of verifications for HDLRB type 2 with 4 SBs (units in kN, cm and s)

α_{K0}	T_{1V}	K_{H0}	K_{V0}	C_H	C_V	D	t_e	S_1	S_2	γ_s	γ_{tot}	P_{cr}/P	σ_t/σ_{tu}
800	0.035	7.69	6149	0.79	3.43	68	19.2	13.7	3.44	1.22	3.81	2.00	0.60
1200	0.034	7.69	9272	0.86	5.02	57	13.2	17.2	4.32	1.77	4.91	2.00	0.96
1600	0.033	7.69	12396	0.86	6.51	57	13.1	21.6	4.33	1.77	4.27	2.63	1.00
2000	0.032	7.69	15521	0.87	7.91	57	13.0	26.7	4.36	1.80	3.84	3.23	1.00

Table 2(b) Properties and results of verifications for HDLRB type 2 with 6 SBs (units in kN, cm and s)

α_{K0}	T_{1V}	K_{H0}	K_{V0}	C_H	C_V	D	t_e	S_1	S_2	γ_s	γ_{tot}	P_{cr}/P	σ_t/σ_{tu}
800	0.030	8.49	6789	0.81	3.24	62	14.5	13.0	4.32	1.61	4.68	2.13	1.00
1200	0.029	8.49	10249	0.82	4.73	64	14.9	17.2	4.26	1.56	3.81	2.86	1.00
1600	0.028	8.49	13714	0.82	6.11	65	15.3	21.6	4.22	1.52	3.27	3.70	1.00
2000	0.028	8.49	17178	0.82	7.66	65	15.6	26.7	4.19	1.50	2.89	4.55	1.00

Table 2(c) Properties and results of verifications for HDLRB type 2 with 8 SBs (units in kN, cm and s)

α_{K0}	T_{1V}	K_{H0}	K_{V0}	C_H	C_V	D	t_e	S_1	S_2	γ_s	γ_{tot}	P_{cr}/P	σ_t/σ_{tu}
800	0.026	9.54	7634	0.76	3.16	69	15.8	13.02	4.39	1.48	3.93	2.70	1.00
1200	0.026	9.54	11488	0.76	4.76	70	16.1	17.15	4.36	1.45	3.29	3.57	1.00
1600	0.025	9.54	15343	0.76	6.11	71	16.4	21.57	4.32	1.42	2.86	4.55	1.00
2000	0.025	9.54	19200	0.76	7.64	71	16.3	26.73	4.33	1.43	2.60	5.56	1.00

Table 3 Properties of the SBs

S4				S6				S8			
α_{K0}	α_{S0}	$\xi_{H,SB}$	$\xi_{H,HDLRB}$	α_{K0}	α_{S0}	$\xi_{H,SB}$	$\xi_{H,HDLRB}$	α_{K0}	α_{S0}	$\xi_{H,SB}$	$\xi_{H,HDLRB}$
800	0.33	4.6%	13.4%	800	0.44	6.4%	11.6%	800	0.55	8.4%	9.6%
1200	0.31	4.4%	13.6%	1200	0.42	6.1%	11.9%	1200	0.54	8.2%	9.8%
1600	0.30	4.2%	13.8%	1600	0.41	5.9%	12.1%	1600	0.54	8.1%	9.9%
2000	0.30	4.2%	13.8%	2000	0.40	5.8%	12.2%	2000	0.53	8.0%	10.0%

reduction that is dependent on sliding velocity) and temperature. The frictional force at the sliding interface of a SB can be expressed as (Dolce *et al.* 2005)

$$F_f = \mu \times P \times Z \tag{11}$$

where Z is a dimensionless hysteretic quantity (Z takes values of ±1 during sliding and less then unity during sticking).

3.3 Friction Pendulum Base-Isolated (FPBI) structures

The alternative of using twenty FPBs acting alone, which are simply assumed with the same effective radius of curvature (R) of the sliding interface, is also taken into account in the design of the FPBI structure shown in Fig. 8. More specifically, two in-plan distributions of maximum axial load capacity (P_{Ed}) are assumed for the FP bearings: FP6.BI structure, with six types of FP bearings (having the same μ_{max} value for all isolators); FP2.BI structure, with

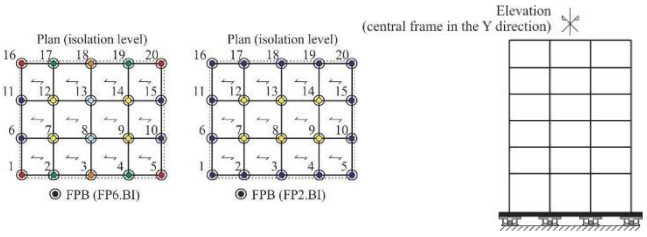

(a) (b)

Fig. 8 FPBI structures: FPBs acting alone

two types of FP bearings (exhibiting six different μ_{max} values), selected with reference to exterior and interior columns.

For constant values of axial load and friction coefficient, the force-displacement behaviour of a FP bearing in the horizontal direction can be represented by a bilinear law (Fig. 9) with a secant stiffness corresponding to the design displacement ($u_{H,d}$)

$$K_e = P\left(1/R + \mu/u_{H,d}\right) \tag{12}$$

related to effective values of the fundamental vibration period and equivalent viscous damping (Petti *et al.* 2013)

$$T_{e,I} = 2\pi\sqrt{\frac{1}{g\left(\frac{1}{R}+\frac{\mu}{u_{H,d}}\right)}};\quad \xi_{e,I} = \frac{2}{\pi}\frac{1}{1+\frac{u_{H,d}}{\mu R}} \tag{13a, b}$$

Moreover, the experimental law derived by a leading world manufacturer of FPBs (FIP 2013) is assumed, to take into account the law of variability of the dynamic-fast friction coefficient with the quasi-permanent gravity load (P_{sd}) applied on the isolators

$$\mu_{max} = 2.5\left(P_{sd}/P_{Ed}\right)^{-0.834} \tag{14}$$

with reference to low-type friction characteristic.

Main properties of the FPBs of FP6.BI and FP2.BI structures are reported in Table 4. The FP system is designed at the ultimate limit state, requiring the fulfilment of the provisions imposed by NTC08: i.e. maximum compression axial load of the FP bearing (P_{sd}) less than its capacity (P_{Ed}); maximum horizontal displacements less than the spectral value; absence of uplift of the FPs.

Finally, the nonlinear force-displacement law of a FPB can be represented considering the restoring (F_r) and

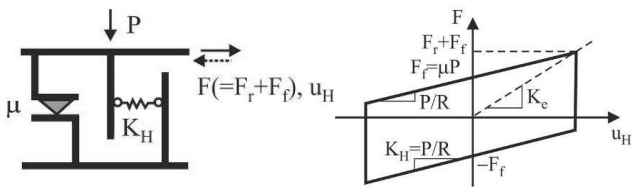

(a) (b)

Fig. 9 Modelling of the base-isolation system for the FPBI structure: FPBs acting alone

Table 4 Properties of the FPBs (units in kN and cm)

FPB	ξ_H	R	P_{sd}	P_{Ed} (FP6.BI)	μ_{max} (FP6.BI)	P_{Ed} (FP2.BI)	μ_{max} (FP2.BI)
1,5,16,20	18%	216	515	970	4.2%	1663	6.7%
2,4,17,19	18%	216	974	1839	4.2%	1663	3.9%
3,18	18%	216	1029	1941	4.2%	1663	3.7%
6,10,11,15	18%	216	1020	1926	4.2%	1663	3.8%
7,9,12,14	18%	216	1458	2753	4.2%	2865	4.4%
8,13	18%	216	1547	2920	4.2%	2865	4.2%

frictional (F_f) forces shown in Fig. 9

$$F = F_r + F_f = K_H u_H + \text{sign}(\dot{u}_H)\mu P \qquad (15)$$

with a lateral restoring stiffness (K_H) and a fundamental vibration period (T_I) of the FPB system independent from the mass

$$K_H = P/R; \quad T_1 = 2\pi\sqrt{R/g} \qquad (16a,b)$$

4. Numerical results

A numerical study is carried out to investigate the main effects produced by the combination of the horizontal and vertical components of near-fault ground motions on the nonlinear response of the (original) fixed-base and (retrofitted) base-isolated structures above described. In the Rayleigh hypothesis, the damping matrix of the superstructure is assumed as a linear combination of the mass and stiffness matrices, assuming a viscous damping ratio in the horizontal ($\xi_{S,H}$) and vertical ($\xi_{S,V}$) direction equal to 2% with reference to the corresponding fundamental vibration periods (i.e., $T_{I,H}$ and $T_{I,V}$, respectively). Seven near-fault ground motions (EQs) available in the Pacific Earthquake Engineering Research center database (PEER 2008) are selected, based on the design hypotheses adopted for the test structure (i.e., subsoil class C and high-risk seismic region). For each ground motion attention is focused on the horizontal component showing the largest PGA value together with the vertical component. The main data of the near-fault EQs are shown in Table 5: i.e., earthquake, recording station, magnitude (M_w), epicentral distance (Δ), peak ground acceleration in the horizontal (PGA_H) and vertical (PGA_V) directions, peak acceleration ratio α_{PGA}. Moreover, different scale factors (SFs) are considered for the normalization of the near-fault EQs with respect to NTC08 acceleration design spectrum, with reference to the fixed-base and base-isolated structures.

More specifically, the selected EQs are normalized with respect to the NTC08 spectrum corresponding to the ultimate life-safety (LS) limit state, considering the Modified Velocity Spectrum Intensity obtained from integration of the velocity (elastic) response spectra in the vertical direction over a defined range of vibration periods (Mollaioli *et al*. 2013). Mean values of the SFs adopted for the selected EQs are reported in Table 6 with reference to fixed-base (FB) and isolated structures (see Figs. 4, 6 and 8).

Table 5 Main data of the selected near-fault ground motions

Earthquake	Recording station	M_w	Δ	PGA_H	PGA_V	α_{PGA}
Imperial Valley, 1979	El Centro D.A.	6.6	5.60 km	0.35 g	0.71 g	2.03
Imperial Valley, 1979	El Centro #7	6.5	3.10 km	0.34 g	0.58 g	1.70
Morgan Hill, 1984	Gilroy #3	6.2	10.3 km	0.19 g	0.40 g	2.04
Coyote Lake, 1979	Gilroy #4	5.7	5.70 km	0.25 g	0.39 g	1.56
Whittier Narrows, 1987	Arcadia	5.9	17.4 km	0.16 g	0.23 g	1.40
Nahanni, 1985	Station I	6.8	6.00 km	0.98 g	2.09 g	2.13
Westmorland, 1981	West. Fire St.	5.6	6.50 km	0.37 g	0.84 g	2.28

Table 6 Mean scale factors for the selected near-fault ground motions

	FB	E800.BI	E1200.BI	E1600.BI	E2000.BI	ES4.BI	ES6.BI	ES8.BI	FP.BI
SF	0.653	0.289	0.319	0.337	0.351	0.434	0.480	0.653	0.653

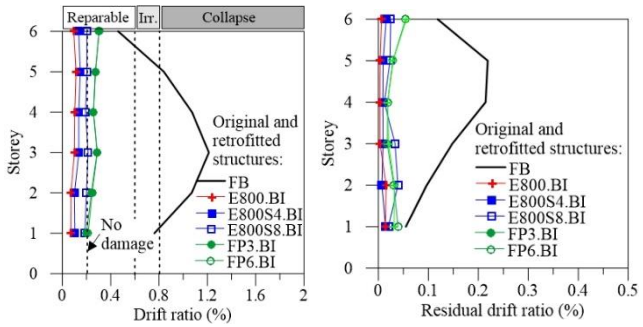

(a) (b)

Fig. 10 Maximum (a) and residual (b) interstorey drift ratio for different elastomeric (α_{K0}=800) and friction (α_{S0}=0.30-1.0) base-isolation systems

Firstly, the storey damage at the LS limit state is investigated in Fig. 10 with reference to the maximum values reached, under the selected EQs, by maximum (Fig. 10(a)) and residual (Fig. 10(b)) interstorey drift ratios (=drift/storey height). The drift ratio thresholds related to different damage levels of r.c. elements in case of nonductile structural systems (Ghobarah 2004), are also reported.

As shown, the FB structure suffers severe damage with partial collapse due to an irregular vertical distribution of the drift ratio (Fig. 10(a)). The insertion of elastomeric (e.g., α_{K0}=800) and friction (e.g., α_{S0}=0.30-1.0) base-isolation systems makes the storey drift distribution almost uniform, reducing the values in the undamaged range for the EBI (i.e., E800.BI) and EFBI (i.e., E800S4.BI, E800S8.BI) structures and moderately (reparable) damaged range for the FPBI (i.e., FP2.BI, FP6.BI) structures. Curves analogous to the previous ones are plotted in Fig. 10(b) to compare the maximum residual drift ratio obtained for the

original (fixed-base) and retrofitted (base-isolated) structures. The residual drift ratio is an important parameter because it represents the irrecoverable part of the interstorey drift, related to damage requiring repair after an earthquake. Note that a highly irregular shape of the residual drift ratio is obtained for the FB structure, while the re-centering properties of HDLRBs and FPBs proves to be very effective for both the EFBI and FPBI structures. Finally, it is interesting to note that maximum effects in terms of storey damage of the base-isolated structures are observed for the highest values of the sliding ratio, which are obtained for the E800S8.BI (i.e., α_{S0}=0.5), FP2.BI and FP6.BI (i.e., α_{S0}=1.0) structures.

Next, to investigate the effects due to the vertical component of the near-fault EQs on r.c. frame members, local structural damage along the building height, in terms of maximum ductility demand of columns (i.e., end sections) and beams (i.e., end, quarter- and mid-span sections), is shown in Figs. 11-12. More specifically, the ductility demand is calculated in terms of curvature, assuming as yielding curvature for the columns the one corresponding to the axial load due to the gravity loads. For sake of brevity, only the results for the central frame along the Y direction (see Fig. 1(a)), having a tributary area for gravity loads greater than those corresponding to the lateral and interior frames, are reported for test structures retrofitted with elastomeric (i.e., α_{K0}=800 in Fig. 11 and α_{K0}=2000 in Fig. 12) and friction (i.e., α_{S0}=0.30-1.0 in Fig. 11 and α_{S0}=0.53-1.0 in Fig. 12) base-isolation systems. As expected, all the base-isolation systems are resulted effective for reducing local damage of r.c. frame members, in comparison with the (original) fixed-base structure. However, unexpected high values of ductility demand are resulted especially at the lower floors, at the end (Fig. 11(b) and Fig. 12(b)) and quarter-span (Fig. 11(c) and Fig. 12(c)) sections of beams. This behaviour is more evident for the EFBI and FPBI structures, whose response in the horizontal direction is like that of a fixed-base structure until the friction threshold imposed by the SBs and FPBs, respectively, is not exceeded. Moreover, it is worth noting the limited influence of the α_{K0} value on the ductility demand to r.c. members of the EBI and EFBI structures. On the other hand, the mid-span sections of the beams (Fig. 11(d) and Fig. 12(d)) undergo increasing ductility demand when assuming an increasing α_{K0} value for the HDLRBs of the EBI and EFBI (especially with four SBs) structures. This behaviour can be explained observing that for rather high values of α_{K0} the superstructure can be considered as a fixed-base structure with reference to the vertical direction. Moreover, a behaviour more similar to that of the original fixed-base structure is obtained in the mid-span sections of the FPBI structures, which are characterized by a sliding ratio α_{S0}=1.0. Analogous results, omitted for the sake of brevity, are obtained considering EBI structures characterized by different values of α_{K0} (i.e., α_{K0}=1200 and 1600 in Tables 1 and 2) and EFBI structures with six SBs (i.e., exhibiting α_{S0}=0.40; see Table 3).

Further results, omitted for sake of brevity, highlight that the base-isolation system of the EFBI structures is characterized by maximum values of γ_s and γ_{tot} greater than those obtained for the EBI structures, but in all the examined cases its failure is not attained under the selected near-fault EQs. Finally, only limited re-centring problems are highlighted for SBs of the E800S8.BI and E2000S8.BI structures and FPBs of FP3.BI and FP6.BI structures, while sufficient restoring capability is obtained for the E800S4.BI and E2000S4.BI structures.

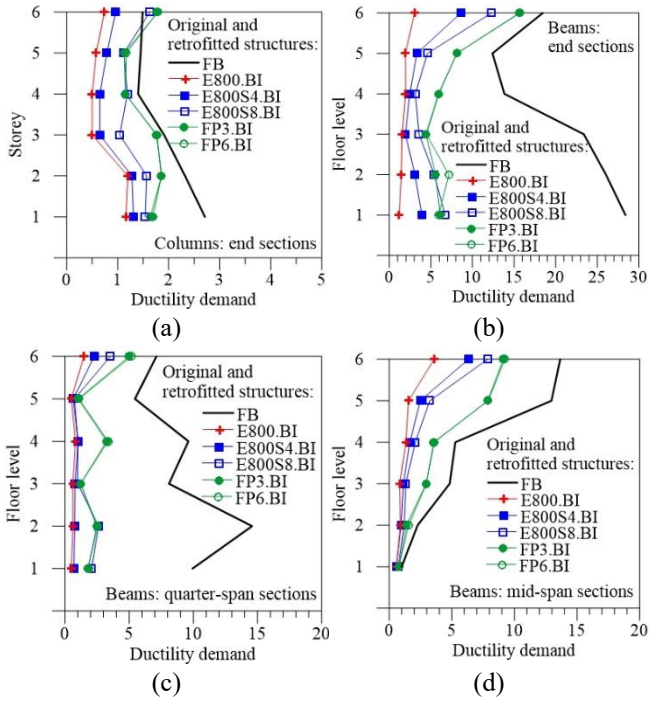

Fig. 11 Ductility demand for elastomeric (α_{K0}=800) and friction (α_{S0}=0.30-1.0) base-isolation systems

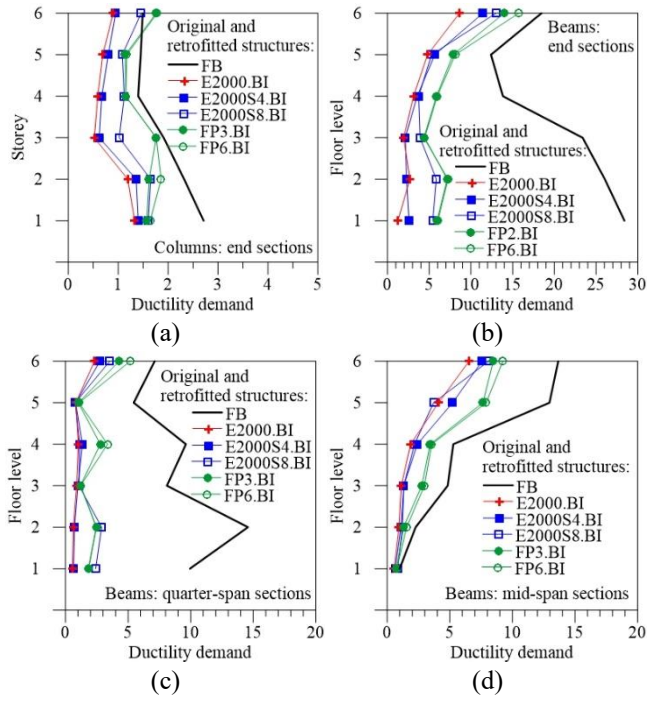

Fig. 12 Ductility demand for elastomeric (α_{K0}=2000) and friction (α_{S0}=0.53-1.0) base-isolation systems

5. Conclusions

The nonlinear dynamic response of an existing six-storey framed building has been studied under near-fault EQs with high values of the acceleration ratio α_{PGA}. Besides the fixed-base (FB) original structure, three cases with different base isolation systems are compared: HDLRBs acting alone; in-parallel combination of HDLRBs and SBs; FPBs acting alone. Different values of the nominal stiffness ratio α_{K0}, for the HDLRBs, and nominal sliding ratio α_{S0}, for the SBs and FPBs (α_{S0}=1), are also considered.

The FB structure suffers severe damage with partial collapse, exhibiting an irregular vertical distribution of the maximum drift ratio, but the insertion of elastomeric and friction base-isolation systems makes the storey drift distribution almost uniform, reducing the values in the undamaged (EBI and EFBI structures) and moderately damaged (FPBI structure) ranges. An irregular shape of the residual drift ratio is obtained for the FB structure, while the re-centering properties of HYDBs and FPBs proves to be very effective for the EFBI and FPBI structures.

All the base-isolation systems are resulted effective for reducing maximum ductility demand of r.c. frame members, in comparison with the FB structure. Unexpected high values of ductility demand are resulted especially at the lower floors, at the end and quarter-span sections of beams. Moreover, the mid-span sections of the beams undergo increasing ductility demand for an increasing α_{K0} value, when the EBI and EFBI structures are considered. Limited re-centring problems are found for the base-isolation systems with SBs (i.e., E800S8.BI and E2000S8.BI structures) and FPBs (i.e., FP2.BI and FP6.BI structures).

Acknowledgements

The present work was financed by Re.L.U.I.S. (Italian network of university laboratories of earthquake engineering), in accordance with "Convenzione D.P.C.-Re.L.U.I.S. 2014-16, WPI, Isolation and Dissipation".

References

Baratta, A., Corbi, I., Corbi, O., Barros, R.C. and Bairrão, R. (2012), "Shaking table experimental researches aimed at the protection of structures subjected to dynamic loading", *Open Constr. Build. Technol. J.*, **6**, 355-360.

Calvi, G.M. (2013), "Choices and criteria for seismic strengthening", *J. Earthq. Eng.*, **17**(6), 769-802.

Chalioris, C.E., Favvata, M.J. and Karayannis, C.G. (2008), "Reinforced concrete beam-column joints with crossed inclined bars under cyclic deformations", *Earthq. Eng. Struct. Dyn.*, **37**(6), 881-897.

Constantinou, M.C., Mokha, A. and Reinhorn, A.M. (1990), "Teflon bearings in base isolation. II: modeling", *J. Struct. Eng.*, **116**(2), 455-474.

De Luca, F. and Verderame, G.M. (2013), "A practice-oriented approach for the assessment of brittle failures in existing reinforced concrete elements", *Eng. Struct.*, **48**, 373-388.

DM96, Italian Ministry of Public Works (1996), "Norme tecniche per le costruzioni in zone sismiche e relative istruzioni", D.M. 16-01-1996 and C.M. 10-04-1997, n. 65/AA.GG.

Dolce, M., Cardone, D. and Croatto, F. (2005), "Frictional behaviour of steel-PTFE interfaces for seismic isolation", *Bull. Earthq. Eng.*, **3**(1), 75-99.

Fagà, E., Ceresa, P., Nascimbene, R., Moratti, M. and Pavese, A. (2016), "Modelling curved surface sliding bearings with bilinear constitutive law: effects on the response of seismically isolated buildings", *Mater. Struct.*, **49**(6), 2179-2196.

Favvata, M.J., Izzuddin, B.A. and Karayannis, C.G. (2008), "Modelling exterior beam-column joints for seismic analysis of RC frame structures", *Earthq. Eng. Struct. Dyn.*, **37**(13), 1527-1548.

Favvata, M.J. and Karayannis, C.G. (2014), "Influence of pinching effect of exterior joints on the seismic behavior of RC frames", *Earthq. Struct.*, **6**(1), 89-110.

FIP Industriale (2013), Catalogue S04. Curved surface sliders, Padova, Italy, http://www.fipindustriale.it.

Foti, D. (2014), "Response of frames seismically protected with passive systems in near-field areas", *Int. J. Struct. Eng.*, **5**(4), 326-345.

Ghobarah, A. (2004), "On drift limits associated with different damage levels", *Proceedings of the International Workshop Performance-Based Seismic Design: Concepts and Implementation*, Bled, Slovenia.

Karayannis, C.G., Chalioris, C.E. and Sirkelis, G.M. (2008), "Local retrofit of exterior RC beam-column joints using thin RC jackets - An experimental study", *Earthq. Eng. Struct. Dyn.*, **37**(5), 727-746.

Karayannis, C.G., Favvata, M.J. and Kakaletsis, D.J. (2011), "Seismic behavior of infilled and pilotis RC frame structures with beam-column joint degradation effect", *Eng. Struct.*, **33**(10), 2821-2831.

Kasalanati, A. and Constantinou, M.C. (2005), "Testing and modeling of prestressed isolators", *J. Struct. Eng.*, **131**(6), 857-866.

Lima, C., Martinelli, E. and Faella, C. (2012), "Capacity models for shear strength of exterior joints in RC frames: state-of-the-art and synoptic examination", *Bull. Earthq. Eng.*, **10**(3), 967-983.

Lomiento, G., Bonessio, N. and Benzoni, G. (2013), "Friction model for sliding bearings under seismic excitation", *J. Earthq. Eng.*, **17**(8), 1162-1191.

Mazza, F. (2015), "Comparative study of the seismic response of RC framed buildings retrofitted using modern techniques", *Earthq. Struct.*, **9**(1), 29-48.

Mazza, F. (2015), "Nonlinear incremental analysis of fire-damaged r.c. base-isolated structures subjected to near-fault ground motions", *Soil Dyn. Earthq. Eng.*, **77**, 192-202.

Mazza, F. (2016), "Effects of near-fault vertical earthquakes on the nonlinear incremental response of r.c. base-isolated structures exposed to fire", *Bull. Earthq. Eng.*, **14**(2), 857-866.

Mazza, F. and Mazza, M. (2016), "Nonlinear seismic analysis of irregular r.c. framed buildings base-isolated with friction pendulum system under near-fault excitations", *Soil Dyn. Earthq. Eng.*, **90**(1), 299-312.

Mazza, F. and Pucci, D. (2016), "Static vulnerability of an existing r.c. structure and seismic retrofitting by CFRP and base-isolation: A case study", *Soil Dyn. Earthq. Eng.*, **84**, 1-12.

Mazza, F. and Vulcano, A. (2010), "Nonlinear dynamic response of r.c. framed structures subjected to near-fault ground motions", *Bull. Earthq. Eng.*, **8**(6), 1331-1350.

Mazza, F. and Vulcano, A. (2012), "Effects of near-fault ground motions on the nonlinear dynamic response of base-isolated r.c. framed buildings", *Earthq. Eng. Struct. Dyn.*, **41**(2), 211-232.

Mazza, F., Mazza, M. and Vulcano, A. (2012), "Nonlinear dynamic response of rc buildings with different base-isolation systems subjected to horizontal and vertical components of

near-fault ground motions", *Open Constr. Build. Technol. J.*, **6**, 346-354.
Mollaioli, F., Lucchini, A., Cheng, Y. and Monti, G. (2013), "Intensity measures for the seismic response prediction of base-isolated buildings", *Bull. Earthq. Eng.*, **11**(5), 1841-1866.
Naeim, F. and Kelly, J.M. (1999) *Design of seismic isolated structures: from theory to practice*, Wiley & S. Ltd., NY.
NTC08 (2008), *Technical Regulations for the Constructions*, Italian Ministry of the Infrastructures. (in Italian)
PEER (2008), "Pacific Earthquake Engineering Research center. Next Generation Attenuation (NGA) database", http://peer.berkeley.edu/peer_ground_motion_database.
Petti, L., Polichetti, F. and Palazzo, B. (2013), "Analysis of seismic performance of fps base isolated structures subjected to near fault events", *Int. J. Eng. Technol.*, **5**(6), 5233-5240.
Ryan, K.L., Kelly, J.K. and Chopra, A.K. (2004), "Experimental observation of axial load effects in isolation bearings", *Proceedings of the 13th World Conference on Earthquake Engineering*, Vancouver, Canada, paper No. 1707.
Sorace, S. and Terenzi, G. (2014), "Motion control-based seismic retrofit solutions of R/C school building designed with earlier Technical Standards", *Bull. Earthq. Eng.*, **12**(6), 2723-2744.
Tsonos, A.G. (2007), "Cyclic load behavior of RC beam-column subassemblages of modern structures", *ACI Struct. J.*, **104**(4), 468-478.
Tsonos A.-D.G. (2010), "Performance enhancement of R/C building columns and beam-column joints through shotcrete jacketing", *Eng. Struct.*, **32**(3), 726-740.
Tsonos, A.-D.G. (2014), "A new method for earthquake strengthening of old R/C structures without the use of conventional reinforcement", *Struct. Eng. Mech.*, **52**(2), 391-403.

AT